Theoretical optimization of the characteristics of ZnO metal-semiconductor-metal photodetectors

Ghania Harzallah* **and Mohamed Remram**

Lemeamed Laboratory, Department of Electronics, University of Mentouri Constantine, Algeria

**Corresponding author: ghan_harzallah@yahoo.fr*

Received December 20, 2010; accepted March 15, 2011; posted online July 11, 2011

A two-dimensional model of a metal-semiconductor-metal (MSM) ZnO-based photodetector (PD) is developed. The PD is based on a drift diffusion model of a semiconductor that allows the calculation of potential distribution inside the structure, the transversal and longitudinal distributions of the electric field, and the distribution of carrier concentration. The ohmicity of the contact has been confirmed. The dark current of MSM PD based ZnO for different structural dimensions are likewise calculated. The calculations are comparable with the experimental results. Therefore, the influence with respect to parameters s (finger spacing) and w (finger width) is studied, which results in the optimization of these parameters. The best optimization found to concur with the experimental results is $s = 16$ μm, $w = 16$ μm, $l = 250$ μm, $L = 350$ μm, where l is the finger length and L is the length of the structure. This optimization provides a simulated dark current equal to 24.5 nA at the polarization of 3 V.

OCIS codes: 040.5160, 250.0250, 160.6000.

doi: 10.3788/COL201109.100401.

Extremely complex, integrated photonic circuits are developed and industrially produced. This is in consideration of the demand for low-cost high-bandwidth circuits, and the demand for knowledge control regarding the manufacturing processes of semiconductor optoelectronic components. The metal-semiconductor-metal (MSM) photodetector (PD) is a good choice in the photo detection field due to the simplicity of manufacture and suitability for monolithic integration[1,2]. Indeed, the planar structure of MSM PD results in an exceptionally small capacity, which is highly desired for high-bandwidth and low-noise performance[3]. Recently, general manufacture of MSM PD used semiconductor materials with wide and direct gaps. The ZnO with direct gap (3.3 eV) has attracted considerable interest because of its excellent electrical properties that allow wide application in high temperatures and high pressures, as well as in the fabrication of components needed to address very high response time[4,5]. Furthermore, ZnO has high sensitivity in ultra-violet detection, making it one of the detectors popularly used for monitoring air quality and gas detection, as well as in military applications[6−8].

In recent years, a significant number of studies have focused on the MSM PD based ZnO, using different metals for interdigitated contacts. Majority of these studies were experimental[9−11], with only a few focusing on the theoretical aspect. The model construction is important in understanding a certain number of physical phenomena that may be difficult to achieve experimentally because of the high cost and time requirement, particularly those of advanced technologies. Controlling transport phenomena in MSM PDs by modelling with numerical methods is especially important in the present case because specific materials such as undoped ZnO are used. Other researchers have developed the subject using simulators, such as COSMOL multiphysics[12,13]. In the present work, a two-dimensional (2D) theoretical model of a MSM-PD-based ZnO is developed, with aluminum as the interdigitated metal contact. The dark current is a point of interest because it provides important electrical properties such as the direct reflection of PD sensitivity. A number of different dimensions of the MSM structure are used to calculate the current. The results are interpreted and discussed to provide an optimum geometry in obtaining a minimum dark current. A comparison with experimental results is performed.

The MSM PD consists of two interpenetrating metal contacts in the form of an interdigitated comb; one is forward biased and the other is reversed biased. The free surface of the semiconductor between the two contacts is the active area for absorbing light for photocurrent generation. Command and control of the electric conduction mechanism make it possible to minimize the dark current. Thus, the conception of a proper design for MSM PD which can detect even the lowest electrical power is possible. The basic layout of the planar MSM PD for simulation is given in Fig. 1.

The metal-semiconductor contacts can be ohmic or Schottky depending on the value of metal work function and the value of the semiconductor affinity. Considering the geometrical symmetry of interdigitated electrodes and facility of calculation, only a unit cell was considered, in which the unit cell lateral boundaries are found in the middle of two adjacent electrodes (Fig. 2).

The proposed model is a 2D physical drift diffusion model based on the Poisson equation, continuity equations, and equations of currents. The expressions are

$$\varepsilon \nabla^2 \psi = -q(p - n + N_{\mathrm{D}}), \quad (1)$$

$$J_{\mathrm{n}} = q\mu_{\mathrm{n}} nE + qD_{\mathrm{n}} \nabla_{\mathrm{n}}, \quad (2)$$

$$J_{\mathrm{p}} = q\mu_{\mathrm{p}} pE - qD_{\mathrm{p}} \nabla_{\mathrm{n}}, \quad (3)$$

$$\frac{\partial n}{\partial t} = \frac{1}{q} \nabla \cdot J_{\mathrm{n}} - R + G_{\mathrm{opt}}, \quad (4)$$

 © 2011 Chinese Optics Letters

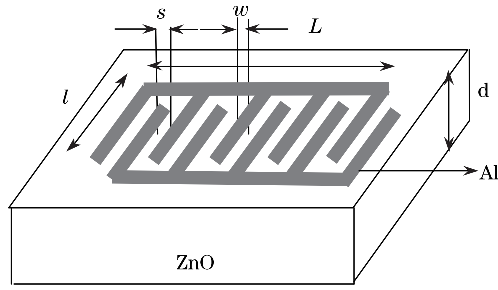

Fig. 1. Layout of basic MSM structure.

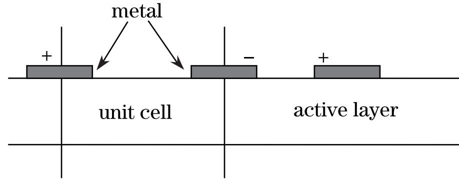

Fig. 2. Unit cell used for simulation.

$$\frac{\partial p}{\partial t} = \frac{1}{q}\nabla \cdot J_{\mathrm{n}} - R + G_{\mathrm{opt}}, \quad (5)$$

where q is the electron charge, u_{n} and u_{p} are the electron mobility and hole mobility, respectively, D_{n} and D_{p} are the diffusion constants of electron and hole, respectively, V is the electrostatic potential, n and p are the concentrations of electrons and holes, respectively, J_{n} and J_{p} are the current densities of electrons and holes, respectively, R is the recombination rate, and G is the generation rate. The phenomenon of generation in the dark was neglected, and work was performed without illumination ($G_{\mathrm{opt}} = 0$). For the recombination, the following expression was used:

$$R = \frac{np - n_i^2}{\tau_{\mathrm{p}}(p + n_i) + \tau_{\mathrm{n}}(n + n_i)}, \quad (6)$$

where n_i is the intrinsic concentration, τ_{n} and τ_{p} are the life time of the electron and the hole, respectively. For the boundary conditions, the Dirichlet condition at semiconductor–metal contact was imposed for the electrostatic potential $V = V_{\mathrm{a}}$(applied voltage). For the other boundaries, the Newman condition for the electrostatic potential and carrier concentrations was applied.

The finite difference method was used for the discretization of the Poisson equation on a uniform mesh. The discretized Poisson equation was solved using the Gauss Seidel method. Subsequently, the potential distribution in the structure was calculated. The values of the potential at the two contacts were taken as initial solution and the values of carrier concentrations $n(x,\ y,\ t)$ and $p(x,\ y,\ t)$ were arbitrarily chosen. The electric field was calculated from the potential in each mesh point using the formula:

$$\overrightarrow{E} = -\overrightarrow{\nabla} V. \quad (7)$$

From the electric field, the electron and hole motilities μ_{u} and μ_{p} were calculated. The diffusion constants of electrons and holes D_{n}, D_{p} were obtained as well. The current densities J_{n} and J_{p} were calculated using Eqs. (2) and (3). The concentrations of carriers were given by the expressions derived from Eqs. (4) and (5) at time $t + \Delta t$, when the J_{n} and J_{p} were determined as

$$n(x, y, ts + \triangle t) = n(x, y, ts) + \int_{ts}^{ts+\triangle t} (\nabla \cdot J_{\mathrm{n}} + G - R)\mathrm{d}t, \quad (8)$$

$$p(x, y, ts + \triangle t) = p(x, y, ts) + \int_{ts}^{ts+\triangle t} (\nabla \cdot J_{\mathrm{p}} + G - R)\mathrm{d}t. \quad (9)$$

The iteration process proceeded according to the algorithm of Fig. 3. After a sufficient number of iterations which resulted in a steady state close to the equilibrium state, the current densities J_{n} and J_{p} obtained were considered as the final results.

The numerical model was applied to study dark current as a function of the polarization of a MSM-PD-based ZnO. Aluminum was used as the interdigitated contact metal. Different dimensions of the structure were used to achieve proper optimization which facilitated the realization of a minimum dark current. The ZnO epitaxial layers used were N-types deposited on a sapphire substrate (0001) by the radio frequency magnetron sputtering technique[14,15]. Table 1 summarizes the parameters used in the simulation[16−18].

Theoretically, an ohmic contact is formed when the value of the semiconductor work function, which is dependent on its affinity, is less than the metal work function[19,20]. The simulation results provided the potential distribution at each mesh point of the structure. Shown in Fig. 4 is the distribution for an applied bias of 3 V. The bias voltage is clearly divided between the two contacts in two equal values, one forward biased and the other reverse biased. This potential is also distributed throughout the structure. Moreover, the distribution

Table 1. Parameters Used for Simulation

Parameter	Value
Affinity of ZnO	4.35 eV
Work Function of Aluminum	4.28 eV
Concentration of Free Carriers	2.5×10^{13} cm^{-3}
Thickness of Active Area	1 μm
Effective Mass of Electron	0.24 m_{o}
Effective Mass of Hole	4.12 m_{o}
Electron Lifetime (τ_{n})	3 μs
Hole Lifetime (τ_{p})	7 μs

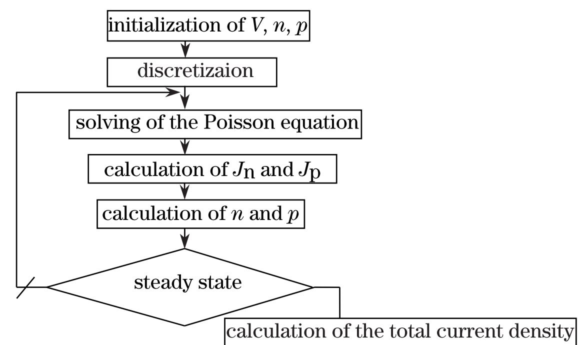

Fig. 3. Algorithm adopted for simulation.

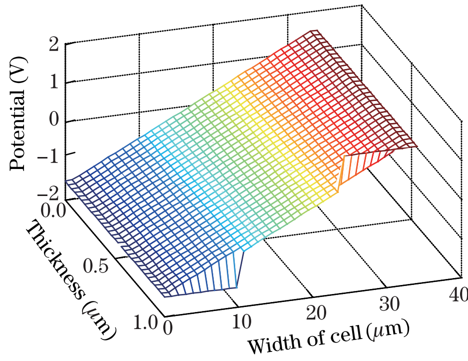

Fig. 4. Distribution of potential inside the MSM PD at 3 V bias.

clearly shows that the contact is ohmic. This result is confirmed in Refs. [21,22].

Figure 5 shows the distribution of transversal component of electric field E_x and longitudinal component of electric field E_y.

At the level of two contacts, the longitudinal and transversal components of electric field have the same absolute values. This confirms the ohmicity of the metal-semiconductor contact (Al-ZnO). The electric field components have maximum values at opposite boundaries of the two adjacent contacts. This indicates that the carrier transport occurs between the two contacts. Hence, the longitudinal component has positive values whereas the transversal component has negative values. The intensity of the electric field is notably high at contact level, and disappears into the rest of the MSM structure. This occurrence has been cited by other authors[12,23]. The use of electric field components in the current equations allows the calculation of current densities J_n and J_p based on the continuity equations. Subsequently, the carrier concentrations n and p were calculated. Figure 6 presents the results. Figures 6(a) and (b) show the distribution of electrons and holes throughout the structure, respectively. Charges accumulate at the interface metal-semiconductor, whereas the variation of these charges is negligible in the rest of the structure. This phenomenon is well known in studies on the ohmic contacts based on semiconductors.

As previously mentioned, the main feature referred to by the simulation is the dark current. The current which was calculated theoretically according to the proposed model was considered as the current density that traverses half the width of the contact finger. The following relationship was applied to calculate the total current (without illumination) through the whole structure:

$$I = 2slNJ, \tag{10}$$

where l is the length of the finger, N is the number of fingers, J is the density of dark current, and s represents the spacing fingers. A bias voltage between 3 and −3 V was applied to obtain the characteristic of the dark current as a function of voltage. This characteristic is obtained for different sizes of geometric parameters of the structure in occurrence, namely w, s, l, and L, which correspond to finger width, finger spacing, finger length, and the length of the structure, respectively. Simulation results were compared with experimental results from Ref. [24] for validation. These experiments were based on four samples with different metal contact geometries. The dimensions of these geometries are compiled in Table 2.

Figure 7 shows the evolution of the experimental dark current as a function of the variation of the bias voltage for different values of the elements of the metal contact geometry. The characteristic $I(V)$ is linear, which implies that the Al–ZnO contact is ohmic. This agrees with previous results. Likewise, the variation of dark current depends mainly on l and L, which define the surface structure. Furthermore, the variation of s and w seems insignificant. When bias voltage v=3, l=500 μm, and L=550 μm, the best dark current obtained is 48 nA.

This current was simulated based on the geometric parameters of the MSM PD structure (L, l, s, w), to confirm the result and find the optimal parameters for a better dark current. The simulation results of samples E1, E2, E3, and E4 were compared with the experimental results. Figure 8 shows the evolution of the experimental dark current and the simulated dark current according to the variation of bias voltage. The simulated dark current shows the same trend as that of the experimental dark current. However, the values of simulations are lower than the experimental values.

Table 2. Values of Different Parameters of the Structure Used for La Simulation

Sample	s(μm)	w(μm)	l(μm)	L(μm)
Sample E1	18	16	500	550
Sample E2	16	14	350	350
Sample E3	14	12	200	300
Sample E4	12	10	150	250

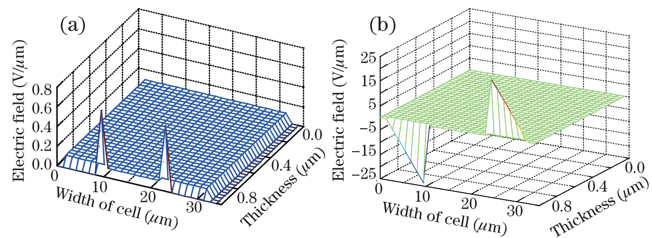

Fig. 5. Distribution of electric field inside the MSM PD at 3 V bias. (a) Longitudinal electric field; (b) transverse electric field.

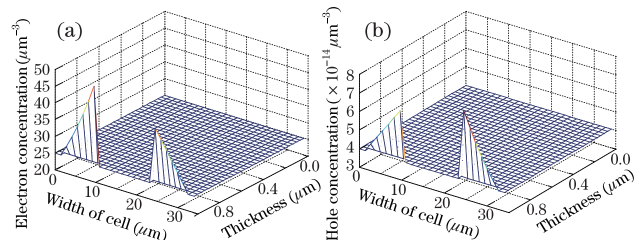

Fig. 6. Distribution of carrier concentration inside the MSM PD at 3 V bias. (a) Electron concentration distribution; (b) hole concentration distribution.

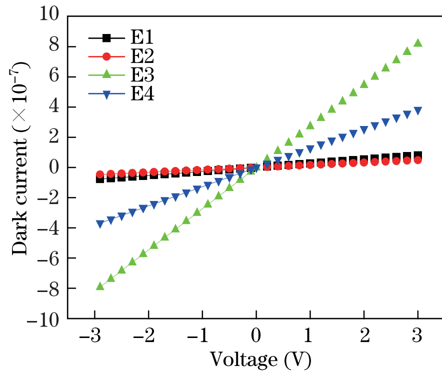

Fig. 7. Experimental dark current as a function of polarization.

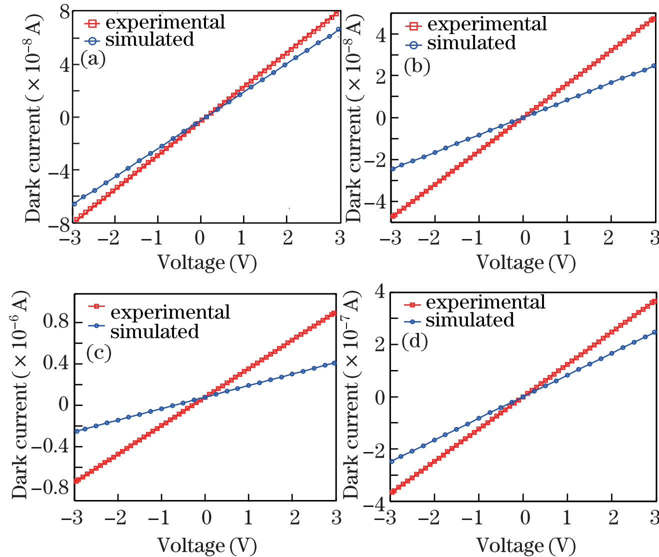

Fig. 8. Dark current as a function of bias voltage for different samples. (a) E1; (b) E2; (c) E3; (d) E4.

The discrepancy is probably due to structural effects, particularly the presence of interface states which were ignored in the model. These interface states orginated from the non-homogeneity and non-uniformity of the surface. Moreover, the additional states resulted from the deposition of metal on the semiconductor. The most noticeable change is the concentration at the semiconductor surface. This can be explained by the existence of a thin layer of n + ZnO at Al–ZnO interface. Aluminum is a well-known donor in ZnO, and thus, it reacts strongly with chalcogenide. Therefore, a very thin layer of highly doped ZnO could appear at the interface of aluminum–ZnO[25]. As an extension of the theoretical study, a structure which adheres to technical contraints on MSM PD size (l=250 μm and L=350 μm) was simulated. A study of the influence of parameters s and w on the dark current has been conducted. We provided variations of the ratio s/w in the interval [0.4, 1.8] because the experimental value of the latter is approximately 1. Figure 9 shows the variation of dark current for l and L mentioned above, based on the variation of s/w.

The dark current increased with the increase of the s/w ratio. Therefore, a low value of the ratio s/w must be chosen to produce low dark current. This requires s to be less than w. On the other hand, the photodetection should be as good as possible. In the present study, the metallization (aluminum) is opaque, thus s must be greater than w. An optimization of s and w is therefore essential. The optimal value is where the ratio s/w equals 1. The optimal parameters achieved a minimum dark current equal 25 nA at 3 V bias. The optimum geometry of the resulting metal structure is s=w=16 μm, l=250 μm, and L=350 μm.

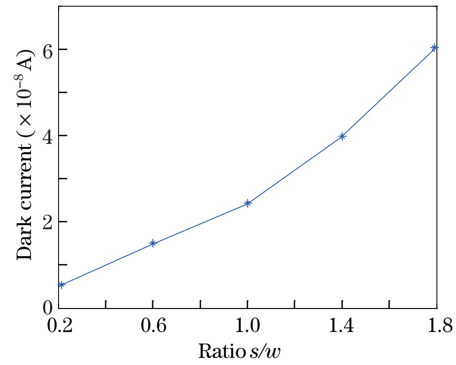

Fig. 9. Dark current as a function of s/w ratio.

In conclusion, a physical model of 2D simulation of a MSM PD based ZnO founded on the drift diffusion model is developed. The basic equations of the model are the Poisson equation, continuity equations, and current equations. This allows the simulation of the dark current component for different dimensions of the metal structure geometry. The simulation results are concurrent with the experimental results. The parameter variation of the metallic geometry contact affects the dark current. The optimization of s/w ratio is crucial in finding the best values for s and w, which simultaneously result in a low dark current and improve the absorption of incident light. The optimized values s= 16 μm, w=16 μm, l=250 μm, and L=350 μm are obtained. The corresponding simulated dark current equal to 24.5 nA at 3 V bias is likewise realized.

References

1. K. Litvin, J. Burm, D. Woodard, W. Schaff, and L. F. Eastman, in *Proceedings of IEEE MTT-S Dig.* **2,** 1063 (1993).
2. S. Y. Chou and M. Y. Liu, IEEE J. Quantum Electron. **28,** 2358 (1992).
3. L. K. Wang, Z. G. Ju, C. X. Shan, J. Zheng, D. Z. Shen, B. Yao, D. X. Zhao, Z. Z. Zhang, B. H. Li, and J. Y. Zhang, Solid State Commun. **149,** 2021 (2009).
4. L. Lai and C. Lee, Mater. Chem. Phys. **110,** 393 (2008).
5. M. Ahmad, C. Pan, J. Zhao, J. Iqbal, and J. Zhu, Mater. Chem. Phys. **120,** 319 (2010).
6. T. K. Lin, S. J. Chang, Y. K. Su, B. R. Huang, M. Fujita, and Y. Horikoshi, J. Crys. Growth **281,** 513 (2005).
7. S. J. Young, L. W. Ji, S. J. Chang, and Y. K. Su, J. Crys. Growth **293,** 43 (2006).
8. S. Liang, H. Sheng, Y. Liu, Z. Huo, Y. Lu, and H. Shen, J. Crys. Growth **225,** 110 (2001).
9. D. Jiang, J. Zhang, Y. Lu, K. Liu, D. Zhao, Z. Zhang, D. Shen, and X. Fan, Solid State Electron. **52,** 679 (2008).
10. Z. Xu, H. Deng, J. Xie, Y. Li, and X. Zu, Appl. Surf. Sci. **253,** 476 (2006).
11. S. J. Young, L. W. Ji, T. H. Fang, S. J. Chang, Y. K. Su,

and X. L. Du, Acta Mater. **55,** 329 (2007).
12. G. Guarino, W. R. Donaldson, M. Mikulics, M. Marso, P. Kordoš, and R. Sobolewski, Solid State Electron. **53,** 1144 (2009).
13. J. Zhang, Y. Yang, L. Lou, and Y. Zhao, Chin. Opt. Lett. **6,** 615 (2008).
14. G. Harzallah, M. Remram, and A. Nehhas, in *Proceedings of 6th Symposium* SiO_2, *Advanced Dielectrics and Related Devices* (2006).
15. G. Harzallah and M. Remram, Matériaux 13 (2006).
16. W. S. Han, Y. Y. Kim, B. H. Kong, and H. K. Cho, Thin Solid Films **517,** 5106 (2009).
17. S. P. Chang, S. J. Chang, Y. Z. Chou, C. Y. Lu. Y. C. Lin, C. F. Kuo, and H. M. Chang, Sensor Actuat A-Phys. **140,** 60 (2007).
18. K. W. Liu, J. G. Ma, J. Y. Zhang, Y. M. Lu, D. Y. Jiang, B. H. Li, D. X. Zhao, Z. Z. Zhang, B. Yao, and D. Z. Shen, Solid State Electron. **51,** 757 (2007).
19. H. Kim and J. Lee, Superlattice Microst. **42,** 255 (2007).
20. J. H. Kim, J. Y. Moon, H. S. Lee, W. S. Han, H. K. Cho, J. Y. Lee, and H. S. Kim, Mater. Sci. Eng. B **165,** 77 (2009).
21. D. Decoster and J. Harari, *Détecteur Optoélectronique* (Hermes Science, Lavoisier, 2002).
22. H. Mathieu, *Physique Des Semiconducteurs et Des Composants Électroniques* (Dunod, Paris, 2001).
23. S. Averine, O. Bondarenko, and R. Sachot, Solid State Electron. **46,** 2045 (2002).
24. A. M. Nahhas, Elektrika **10,** 1 (2008).
25. Y. Dong and L. J. Brillson, J. Electron. Mater. **37,** 743 (2008).